PAPER

Check for updates

High-symmetry cage-like molecule N20(C2B2)30: computational insight into its bonding and reactivity†

Miaorun Zhang, Lin Zhang, [ID] Zexing Cao [ID] and Yi Zhao [ID] *

On the basis of density functional theory (DFT) calculations and AIMD simulations, a novel I_h-symmetry cage-like molecule $N_{20}(C_2B_2)_{30}$ is constructed and characterized computationally. It is found that $N_{20}(C_2B_2)_{30}$ is structurally similar to fullerene C_{20}, but it has high thermodynamic and kinetic stability. The designed $N_{20}(C_2B_2)_{30}$ exhibits strong chemical reactivities, including reactivities for the Diels–Alder reaction with butadiene (C_4H_6) and cyclopentadiene (C_5H_6), as well as for the [3+2] addition reaction with diazomethane (N_2CH_2). In addition, the presence of the boron site and the inverted C=C bond with the charge-shift (CS) bonding in $N_{20}(C_2B_2)_{30}$ make it quite active not only for cycloaddition reactions but also for capture of small molecules (*e.g.* H_2, CO, NO, and NO_2). Once $N_{20}(C_2B_2)_{30}$ complexes with a transition metal (TM) ion, the resultant complexes $(TM)N_{20}(C_2B_2)_{30}^+$ (TM = Cu, Ag, and Au) can bind inactive CO_2 and N_2O at the TM site. Furthermore, $AuN_{20}(C_2B_2)_{30}^+$ is able to effectively separate CO_2 and N_2O. Owing to its unique porous structure and reactivity as well as high stability, $N_{20}(C_2B_2)_{30}$ may further enrich the diversity of a highly symmetrical molecular family.

1. Introduction

Highly symmetrical molecules with I_h symmetry can be traced back to *closo*-$[B_{12}H_{12}]^{2-}$, as reported both experimentally and theoretically.[1–3] Owing to its perfect structure and stable physicochemical properties in the closed borane family, this *closo*-$[B_{12}H_{12}]^{2-}$ has begun to play important roles in medicine, energetic materials, new energy, environmental management and optoelectronic materials.[4] In 1985, another kind of soccer-like cage C_{60} with I_h symmetry was reported by Kroto *et al.*[5] Henceforth, there has been long standing interest in using C_{60} in experimental and theoretical domains due to its perfect symmetry and applications in electrochemistry, organic chemistry, nanoscience, nanotechnology, and so on.[6–9] Previous studies have shown that C_{60} can act as a dienophile to undergo a cycloaddition reaction because of its C=C double bond character. Moreover, the Diels–Alder reactions of C_{60} with the derivatives of butadiene and cyclopentadiene, as well as the [3+2] cycloadditions of C_{60} with N_2CR_2 and ONCR are favorable to occur as usual across a 6,6-bond of C_{60}.[10–13] Recently, the

aggregation of Ti atoms on the surface of C_{60} enables it as a potential hydrogen storage material.[14] A C_{60}-modified gold electrode is employed for the determination of dopamine in the excess of ascorbic acid using square-wave voltammetry.[15] C_{60}-buffered Cu/SiO_2 can decrease the energy barriers to effectively synthesize ethylene glycol (EG) under ambient pressure conditions.[16] Thus, C_{60} has been broadly applied in designing functional materials.

Besides *closo*-$[B_{12}H_{12}]^{2-}$ and C_{60}, some molecules and clusters with I_h symmetry are also reported experimentally or theoretically, such as B_{80},[17] $C_{60}H_{60}$, $C_{60}F_{60}$, $Si_{20}H_{20}$, $Si_{60}H_{60}$, and so on.[18,19] The edges of high symmetry molecules and clusters mentioned above are normal B–B, C–C, and Si–Si bonds. Inspired by the synthesis methods of covalent organic frameworks (COFs),[20] we wonder whether high-symmetry cages with linkers on the edges can be obtained by the $[C_3+C_2]$ topology. Herein, a type of high-symmetry cage $N_{20}(C_2B_2)_{30}$, mimicking fullerene C_{20} composed of C_2 and C_3 building blocks, is constructed using C_2B_2 linkers and N nodes, as illustrated in Fig. 1, in which C_2B_2 is taken from the molecule $C_2B_2H_2$ reported experimentally in 2017.[21]

State Key Laboratory of Physical Chemistry of Solid Surfaces, Collaborative Innovation Center of Chemistry for Energy Materials, Fujian Provincial Key Laboratory of Theoretical and Computational Chemistry, and Department of Chemistry, College of Chemistry and Chemical Engineering, Xiamen University, Xiamen 361005, Fujian, People's Republic of China. E-mail: yizhao@xmu.edu.cn
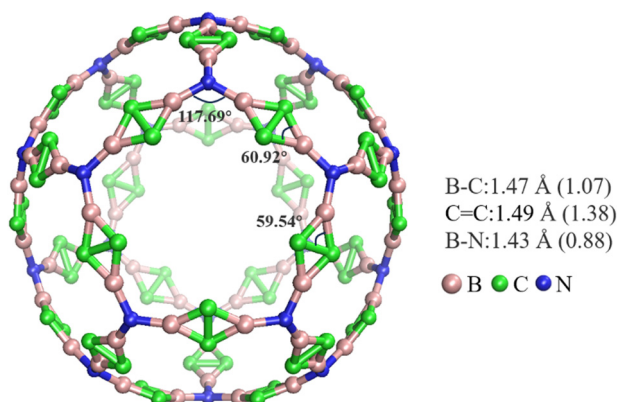† Electronic supplementary information (ESI) available. See DOI: https://doi.org/10.1039/d4cp04653f

2. Computational methods

The geometry optimization of $N_{20}(C_2B_2)_{30}$ and small molecules (H_2, CO, NO, NO_2, CO_2, N_2O, C_4H_6, C_5H_6, and N_2CH_2), as well as

Fig. 1 The optimized structure of $N_{20}(C_2B_2)_{30}$, as well as selected bond lengths, bond angles, and calculated Wiberg bond indices (WBIs, in bracket) are presented. Color scheme: B atom (in pink), C atom (in green), and N atom (in blue).

the corresponding molecular complexes is performed by using the DFT/M06-2X method,[22] in combination with the SDD basis set[23] for Cu, Ag, and Au atoms and the 6-31G(d,p) basis set[24] for the non-metallic atoms. Vibrational frequencies of the studied molecules are calculated at the same level of theory to confirm the true minima on the potential energy surfaces (PESs). The adsorption energies of small gas molecules are estimated by the difference in the total energies of their respective constituents, including the zero-point energy (ZPE) correction and the basis set superposition error (BSSE) correction.[25] The Wiberg bond indices (WBIs) are derived *via* the natural bond orbital (NBO) analysis.[26] The electron density (ρ) and Laplacian values ($\nabla^2\rho$) of certain chemical bonds are calculated using the Multiwfn 3.8 program.[27] Key molecular orbital analysis and the pore diameter of $N_{20}(C_2B_2)_{30}$ can be exported and visualized by using the Multiwfn 3.8 program[27] and VMD 1.9.4 software,[28] respectively. Nucleus independent chemical shifts (NICS) at the centers of the three-membered rings of CCB in $N_{20}(C_2B_2)_{30}$ are calculated using the gauge-independent atomic orbital (GIAO) method.[29] All the above calculations are performed with the Gaussian16 program.[30]

Ab initio molecular dynamics (AIMD) simulations with $N_{20}(C_2B_2)_{30}$ are carried out with the Vienna ab initio simulation package (VASP) program,[31] where the core and valence electrons are represented by using the projector augmented wave (PAW)[32] method and plane-wave basis functions with a kinetic energy cut-off of 520 eV. The generalized gradient approximation (GGA) with the Perdew–Burke–Ernzerhof (PBE)[33] exchange–correlation functional is used in the AIMD calculations. The finite temperature simulations of the dynamic properties are performed at temperatures 298 and 600 K using the exact Hellmann–Feynman forces and applying the statistics of the canonical ensemble to the motion of atomic nuclei by means of a Nosé thermostat.[34] Newton's equations of motion are integrated using the Verlet algorithm[35] with a time step of 1 fs, and the total duration is 10 ps. $N_{20}(C_2B_2)_{30}$ is confined in a cubic box of $25 \times 25 \times 25$ Å, and a vacuum distance of more than 10 Å is set to keep the interactions between the molecules in the adjacent boxes

negligible. The Brillouin-zone sampling is restricted to the Γ-point. The geometry optimization is performed *via* a conjugate gradient algorithm until the residual forces acting on atoms are less than 0.1 eV Å^{-1}.

The thermodynamic stability of a molecule can generally be measured by its cohesive energy. Generally, the greater the cohesive energy, the better the stability. The cohesive energy of $N_{20}(C_2B_2)_{30}$ is computed as follows

$$E_c = \left[E_{(tot)} - \left\{ xE_{(B)} + yE_{(C)} + zE_{(N)} \right\} \right] / n$$

where E_c is the calculated cohesive energy, $E_{(tot)}$, $E_{(B)}$, $E_{(C)}$, and $E_{(N)}$ are the total energies of $N_{20}(C_2B_2)_{30}$, B, C, and N atoms, respectively, x, y, and z are the numbers of atoms B, C, and N, respectively, and n is the total number of all atoms in $N_{20}(C_2B_2)_{30}$.

3. Results and discussion

3.1. Structure and stability of $N_{20}(C_2B_2)_{30}$

The optimized structure of the novel high-symmetry cage-like molecule $N_{20}(C_2B_2)_{30}$, as well as its key lengths and WBIs are shown in Fig. 1. Notably, this molecule is structurally similar to fullerene C_{20}, *i.e.* this molecule contains twelve regular pentagons (see Fig. S1 in the ESI†), in which twenty vertexes are nitrogen atoms and thirty edges are rhombus C_2B_2 units. In contrast to fullerene C_{20},[36–38] the optimized $N_{20}(C_2B_2)_{30}$ with I_h symmetry has the minimum on the PES without any imaginary frequency and Jahn–teller distortion. In addition, the lengths of B–N, B–C, and inverted C=C bonds in $N_{20}(C_2B_2)_{30}$ are 1.43, 1.47, and 1.49 Å, respectively. The C=C bonds in $N_{20}(C_2B_2)_{30}$ are inverted compared with the C=C bond in ethylene, thus, we describe the C=C bond to be the inverted C=C bond. The corresponding WBIs of the B–N, B–C, and inverted C=C bonds are 0.88, 1.07, and 1.38, respectively. Thus, the inverted C=C bond has double bond character which is consistent with B-heterocyclic carbene (BHC), double B-heterocyclic carbene (DBHC), and Si, B-heterocyclic carbene (SiBHC),[39–42] while the B–N and B–C are single bonds. Moreover, the key occupied molecular orbitals (MOs, HOMO−4 to HOMO) involving C=C bonds of $N_{20}(C_2B_2)_{30}$ are evaluated in order to gain insights into its electronic properties, as shown in Fig. S2 (see the ESI†). It is found that these MOs are formed by the sp^2 hybrid orbital of carbon atoms in the C=C bonds, which is well consistent with the reported BHCs, DBHCs, and SiBHCs. Thus, the inverted C=C in $N_{20}(C_2B_2)_{30}$ contains one π bond and one charge-shift (CS) bond.[39–44]

In order to compare the size of $N_{20}(C_2B_2)_{30}$ and C_{60}, we optimize the structure of C_{60} using the M06-2X/6-31G(d,p) approach. Additionally, the pore diameters of the cavity of $N_{20}(C_2B_2)_{30}$ and C_{60} are calculated using the Multiwfn 3.8 program and are shown in Fig. S3 (see the ESI†). The computational results show that the pore diameter of $N_{20}(C_2B_2)_{30}$ is 11.29 Å, which is approximately three times as large as that of C_{60} (3.68 Å). Calculated cohesive energy of $N_{20}(C_2B_2)_{30}$ is −6.00 eV per atom, indicating that it has relatively high

This journal is © the Owner Societies 2025

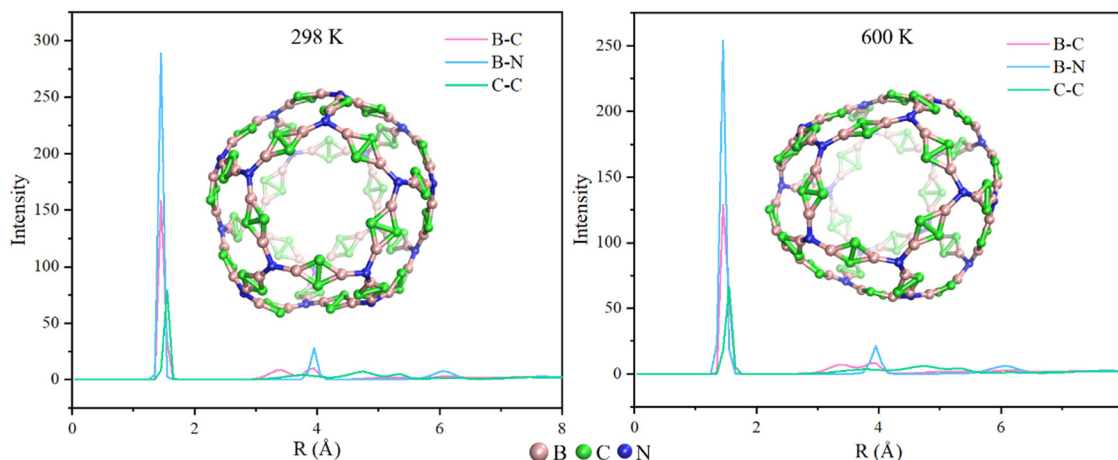*Phys. Chem. Chem. Phys.*, 2025, **27**, 4246–4252 | **4247**

Fig. 2 Radial distribution of interatomic distances at 298 and 600 K. Color scheme: B atom (in pink), C atom (in green), and N atom (in blue).

thermodynamic stability. To further confirm the chemical stability of $N_{20}(C_2B_2)_{30}$, AIMD simulations of $N_{20}(C_2B_2)_{30}$ are performed at T = 298 and 600 K and the specific details are shown in Fig. 2. The structure of $N_{20}(C_2B_2)_{30}$ has no significant changes at 298 and 600 K for 10 ps. According to the radial distribution of interatomic distances, it is suggested that during a 10 ps of AIMD simulation at both 298 and 600 K, the stability of the backbone of $N_{20}(C_2B_2)_{30}$ still remains unchanged. Additionally, all of the B–N, B–C, and C–C bonds of $N_{20}(C_2B_2)_{30}$ are not broken at T = 298 and 600 K during AIMD simulations for 10 ps. Thus, $N_{20}(C_2B_2)_{30}$ has high kinetic stability.

A previous study shows that $C_2B_2H_2$ has the aromatic character according to the NICS(0) and NICS(1) values at the ring center of the three-membered CCB moiety in $C_2B_2H_2$.[21] The NICS(0) and NICS(1) values (inside and outside of the cage) of $N_{20}(C_2B_2)_{30}$ are calculated and shown in Fig. S4 (see the ESI†). It is shown that the NICS(0) value of $N_{20}(C_2B_2)_{30}$ is −17.49, and the NICS(1) values of inside and outside of the cage of $N_{20}(C_2B_2)_{30}$ are −21.32 and −15.30, respectively. Note that the NICS(1) value inside the cage is close to that of $C_2B_2H_2$ molecules,[21] indicating that $N_{20}(C_2B_2)_{30}$ also possesses aromatic character.

3.2. Cycloaddition reaction of $N_{20}(C_2B_2)_{30}$

BHCs, DBHCs, and SiBHCs can behave as dienophiles to undergo Diels–Alder reactions with dienes due to their C=C bond character.[39,40,42] Herein, in order to investigate the reactivity of the C=C bond, the mechanism for the Diels–Alder reactions of $N_{20}(C_2B_2)_{30}$ with butadiene and cyclopentadiene is investigated. The predicted relative free energy profiles of the two Diels–Alder reactions, along with the optimized structures of transition states and products for analyzing the formation of chemical bonds, are shown in Fig. 3. Note that Diels–Alder reaction of $N_{20}(C_2B_2)_{30}$ with butadiene is exothermic and yields the product (**PC1**) *via* the transition state (**TS1**) with a free energy barrier of 20.9 kcal mol^{-1} and an energy release of 48.0 kcal mol^{-1}, which is similar to the addition reaction of BHCs with butadiene.[40] In the Diels–Alder reaction of

$N_{20}(C_2B_2)_{30}$ with cyclopentadiene, a loose intermolecular complex (**RC**) is formed at first, and then the reaction undergoes the transition state (**TS2**) to generate the product (**PC2**), which is consistent with the Diels–Alder reaction of fullerene C_{60} with cyclopentadiene.[45] The free energy barrier for the Diels–Alder reaction of $N_{20}(C_2B_2)_{30}$ with cyclopentadiene is 20.6 kcal mol^{-1}, and the Gibbs free energies of the reaction ΔG is −15.5 kcal mol^{-1}. Clearly, the Diels–Alder reactions of $N_{20}(C_2B_2)_{30}$ with butadiene and cyclopentadiene are feasible, both thermodynamically and kinetically.

The [3+2] cycloaddition reaction of C_{60} as well as its derivatives towards N_2CH_2 undergo either thermal or photochemical loss of dinitrogen to give $C_{60}CH_2$.[13] Here, the mechanism for the [3+2] cycloaddition reaction of $N_{20}(C_2B_2)_{30}$ with N_2CH_2, including loss of dinitrogen, is illustrated in Fig. 4. It is revealed that the [3+2] cycloaddition proceeds to an intermediate (**IM**) through the transition state (**TS3**) with an energy barrier of 14.6 kcal mol^{-1} and an energy release of 25.8 kcal mol^{-1}. Thus, the [3+2] cycloaddition is feasible both thermodynamically and dynamically. Followed by the release of N_2, *i.e.*, $N_{20}(C_2B_2)_{30}N_2$-CH_2 (**IM**) → $N_{20}(C_2B_2)_{30}CH_2$ (**PC3**) + N_2, the final product $N_{20}(C_2B_2)_{30}CH_2$ (**PC3**) of the [3+2] cycloaddition reaction, containing a 3, 4-boratricyclo[1.1.1]pentane, is formed, and the overall Gibbs free energies of the reaction ΔG is −47.6 kcal mol^{-1} relative to the initial reactants, showing the [3+2] cycloaddition is quite feasible, both thermodynamically and kinetically.

The lengths (WBIs) of the C1–C2 bond in **PC1**, **PC2**, **IM**, and **PC3** are 1.73 (0.66), 1.69 (0.74), 1.68 (0.72), and 1.73 Å (0.39), respectively. Thus, the C1–C2 bond is a weak single bond, as found in the products of the Diels–Alder reaction of BHCs.[40]

We have further investigated the reaction mechanism of the successive addition of three butadiene molecules to $N_{20}(C_2B_2)_{30}$. The results show that the free energy barriers at different stages of addition remain essentially unchanged, and the reaction exhibits sustained exergonicity, although the trend of exergonicity slows down. Therefore, it can be inferred that $N_{20}(C_2B_2)_{30}$ may undergo successive addition with butadiene molecules until saturation (see Fig. S5 in the ESI†). In addition, we have compared the
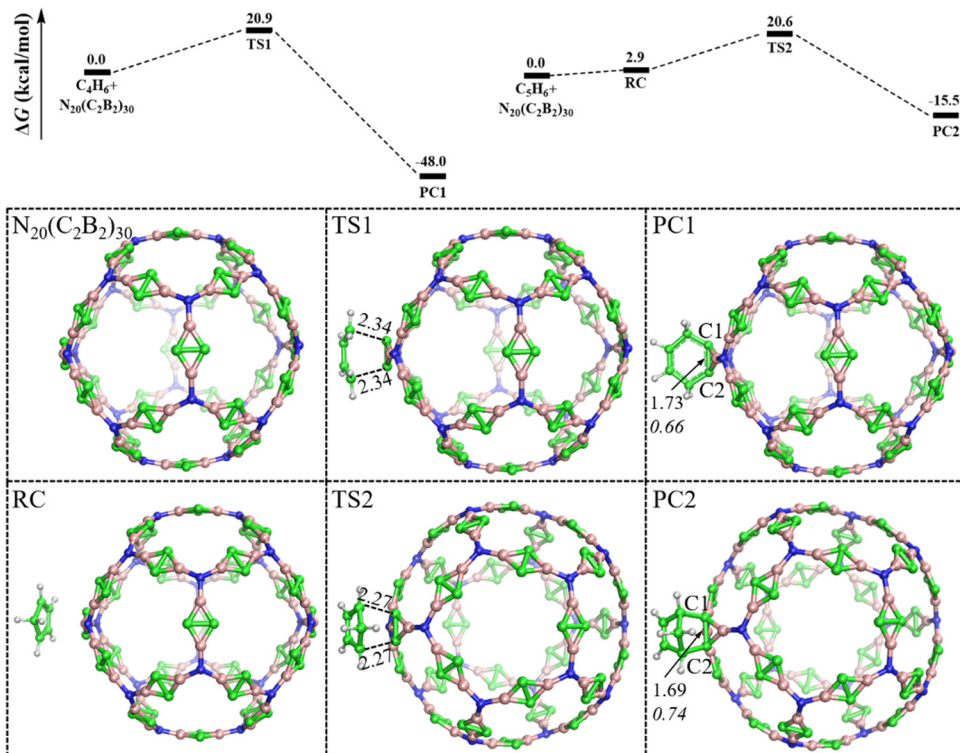
4248 | *Phys. Chem. Chem. Phys.*, 2025, **27**, 4246–4252

This journal is © the Owner Societies 2025

Fig. 3 The predicted relative free energy profiles (in kcal mol^{-1}) for the Diels−Alder reactions of $N_{20}(C_2B_2)_{30}$ with butadiene and cyclopentadiene are shown. Optimized structures, key bond lengths (Å, in plain), and WBIs (in italic). Color scheme: H atom (in white), B atom (in pink), C atom (in green), and N atom (in blue).
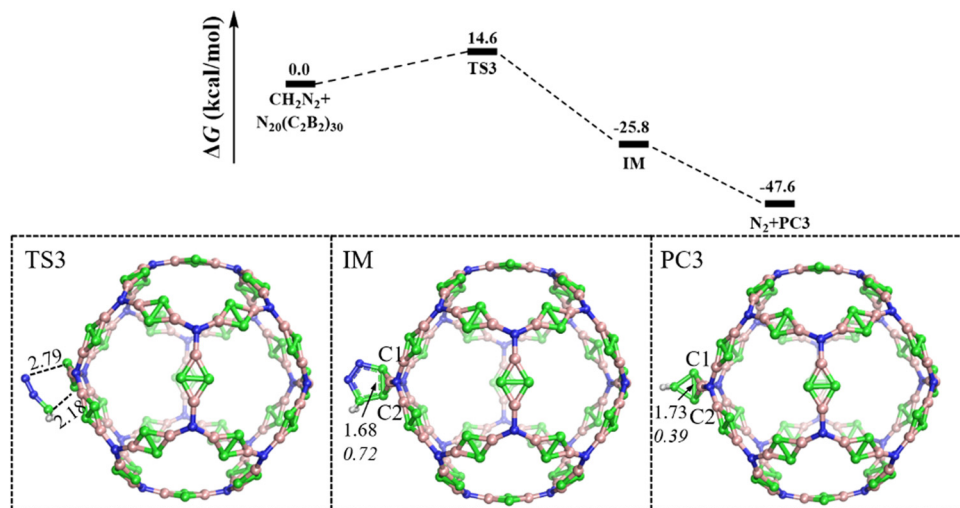

Fig. 4 The predicted relative free energy profile (in kcal mol^{-1}) for the [3+2] cycloaddition of $N_{20}(C_2B_2)_{30}$ with diazomethane is shown. Optimized structures, key bond lengths (Å, in plain), and WBIs (in italic). Color scheme: H atom (in white), B atom (in pink), C atom (in green), and N atom (in blue).

addition reaction activities of the C=C bonds in the exohedral and endohedral additions of the cluster with butadiene. The results indicate that both have comparable addition energy barriers. However, it should be noted that due to the spatial effects within the cluster, the stability of the endohedral addition product is slightly lower than that of the corresponding exohedral product (see Fig. S6 in the ESI†).

3.3. Binding interactions of $N_{20}(C_2B_2)_{30}$ and its ionic complexes with small molecules

Due to the CS bonding character of the inverted C=C bond in $N_{20}(C_2B_2)_{30}$, the carbon atoms can serve as the active sites to bind small molecules. Accordingly, the binding behaviors of $N_{20}(C_2B_2)_{30}$ toward small gas molecules, such as H_2, CO, NO, and NO_2, are considered here. Optimized structures of

This journal is © the Owner Societies 2025

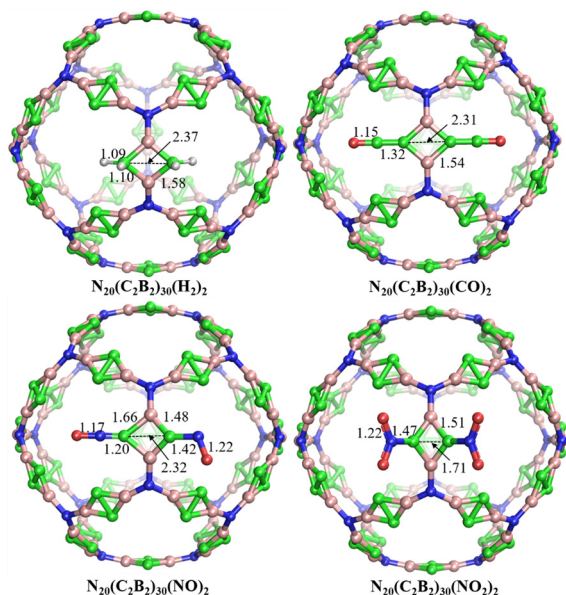*Phys. Chem. Chem. Phys.*, 2025, **27**, 4246−4252 | **4249**

Fig. 5 The complexes of $N_{20}(C_2B_2)_{30}$ with small gas molecules H_2, CO, NO, and NO_2 are shown. Selected bond lengths are given in Å. Color scheme: H atom (in white), B atom (in pink), C atom (in green), N atom (in blue), and O atom (in red).

complexes $N_{20}(C_2B_2)_{30}(H_2)_2$, $N_{20}(C_2B_2)_{30}(CO)_2$, $N_{20}(C_2B_2)_{30}(NO)_2$, and $N_{20}(C_2B_2)_{30}(NO_2)_2$ are illustrated in Fig. 5, and the vibrational analysis reveals that they are all stable without any imaginary frequency. In addition, the evaluated binding energies of $N_{20}(C_2B_2)_{30}$ with H_2, CO, NO, and NO_2 are −3.96, −3.16, −1.72, and −2.57 eV, respectively, indicating that $N_{20}(C_2B_2)_{30}$ can effectively capture H_2, CO, NO, and NO_2. Moreover, since the binding energies are significantly different from each other, $N_{20}(C_2B_2)_{30}$ might be used to separate H_2, CO, NO, and NO_2.

Every carbon atom of the C_2B_2 unit in $N_{20}(C_2B_2)_{30}(H_2)_2$ and $N_{20}(C_2B_2)_{30}(CO)_2$ forms two C–H bonds with H_2 and a C≡CO bond with CO, respectively, resulting in the cleavage of the inverted C≡C bond of $N_{20}(C_2B_2)_{30}$. Interestingly, C≡N (left) and C–N (right) in $N_{20}(C_2B_2)_{30}(NO)_2$ are obviously different with the bond lengths of 1.20 and 1.42 Å, respectively. In order to better understand the bonding nature, the natural bond orbital analysis of $N_{20}(C_2B_2)_{30}(NO)_2$ is performed. As seen from Fig. S7 (see the ESI†), there is a significant electron transfer from the N_1 atom to the C_2 atom, resulting in the C_2 atom with a net negative charge of −0.64. The 2p orbitals of the left O, N, and C atoms form a linear structure with Π_2^2 and Π_3^4 bonds when the N atom loses an electron. In contrast, the 2p orbitals of the right O, N and C atoms form a V-like structure with the Π_3^4 bond when the C atom accepts an electron. The lengths of two N≡O bonds in $N_{20}(C_2B_2)_{30}(NO)_2$ are around 1.20 Å. Two carbon atoms in the C_2B_2 unit in $N_{20}(C_2B_2)_{30}(NO_2)_2$ form two C–N bonds and an inverted C–C bond, and the latter bears a weak π bond character with a distance of 1.71 Å. Thus, $N_{20}(C_2B_2)_{30}$ accommodates two NO_2 through the covalent form of the CS bond of the inverted C···C.

In particular, due to the empty $2p_z$ orbital of the boron atom in $N_{20}(C_2B_2)_{30}$, boron atoms may bind CO through a dative
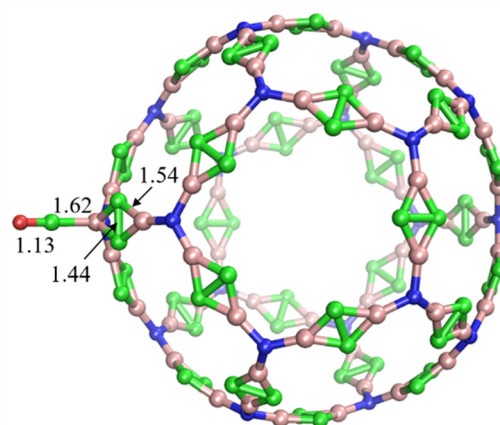

Fig. 6 The adsorption of CO at the B site of $N_{20}(C_2B_2)_{30}$ is shown, where key bond lengths are given in Å. Color scheme: B atom (in pink), C atom (in green), N atom (in blue), and O atom (in red).

bond interaction. The optimized structure of the binding complex $N_{20}(C_2B_2)_{30}(CO)$ is depicted in Fig. 6, and it is a minimum on the PES predicted by the frequency analysis. The calculated adsorption energy of $N_{20}(C_2B_2)_{30}$ + CO → $N_{20}(C_2B_2)_{30}CO$ is −0.02 eV, suggesting that the boron atom in $N_{20}(C_2B_2)_{30}$ is also an active site for CO adsorption.

Although it can bind with the aforementioned small molecules, $N_{20}(C_2B_2)_{30}$ cannot effectively bind with CO_2 and N_2O. Note that a zeolite recently reported can be used to separate CO_2 and N_2O through the Ag^+ site.[46] The carbon atoms of the inverted C≡C bond in $N_{20}(C_2B_2)_{30}$ can coordinate to the transition metal (TM) to form a complex $(TM)N_{20}(C_2B_2)_{30}$.[39] Interestingly, it is found that the newly generated $(TM)N_{20}(C_2B_2)_{30}^+$ (TM = Cu, Ag, and Au) could capture CO_2 and N_2O. The optimized structures of $(TM)N_{20}(C_2B_2)_{30}^+$, $(CO_2)(TM)N_{20}(C_2B_2)_{30}^+$, and $(N_2O)(TM)N_{20}(C_2B_2)_{30}^+$, and the corresponding geometric parameters are illustrated in Fig. 7. Note that TM in $(TM)N_{20}(C_2B_2)_{30}^+$ is coordinated with the terminal C atoms of three inverted C≡C units. Specifically, Cu^+ in $CuN_{20}(C_2B_2)_{30}^+$ binds with CO_2 and N_2O through the interaction of their O and N atoms with Cu, where the newly formed Cu–O or Cu–N bond replaces one Cu–C bond connected to the inverted C≡C unit. Differing from $CuN_{20}(C_2B_2)_{30}^+$, the formation of the TM–O/N bond in $(TM)N_{20}(C_2B_2)_{30}^+$ in (TM = Ag and Au) may weaken the Cu–C (inverted C≡C) bond to some extent. Calculated binding energies for $(TM)N_{20}(C_2B_2)_{30}^+$ + CO_2 → $(CO_2)(TM)N_{20}(C_2B_2)_{30}^+$ (TM = Cu, Ag, and Au) are −0.65, −0.38, and −0.09 eV, respectively. Similarly, the binding energies for $(TM)N_{20}(C_2B_2)_{30}^+$ + N_2O → $(N_2O)(TM)N_{20}(C_2B_2)_{30}^+$ (TM = Cu, Ag, and Au) are −0.68, −0.34, and −0.21 eV, respectively. Here the predicted binding energies of CO_2 and N_2O bound at the Ag^+ site of $AgN_{20}(C_2B_2)_{30}^+$ are well consistent with those of these small molecules bound at the Ag^+ site of the reported zeolite.[46] Accordingly, the introduction of transition metal ions can remarkably enhance the capability of $N_{20}(C_2B_2)_{30}$ toward the binding of inactive molecules, such as CO_2 and N_2O. Furthermore, the adsorption energy difference of 0.12 eV between $AuN_{20}(C_2B_2)_{30}^+$ with CO_2
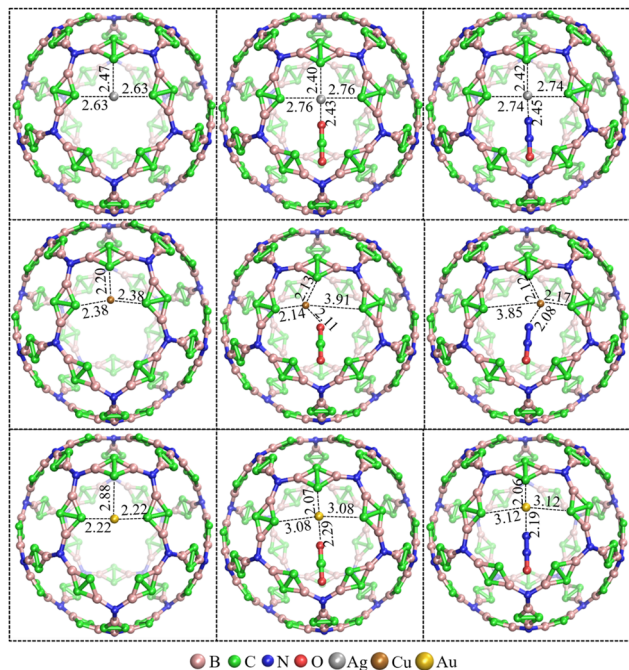
4250 | Phys. Chem. Chem. Phys., 2025, 27, 4246–4252

This journal is © the Owner Societies 2025

Fig. 7 The optimized complexes of $AgN_{20}(C_2B_2)_{30}^+$, $CuN_{20}(C_2B_2)_{30}^+$, and $AuN_{20}(C_2B_2)_{30}^+$ with CO_2 and N_2O, where key bond lengths are given in Å. Color scheme: B atom (in pink), C atom (in green), N atom (in blue), O atom (in red), Ag atom (in silver), Cu atom (in copper), and Au atom (in gold).

and N_2O indicates that these two gas molecules can be effectively separated. In order to better understand the interaction between TM (TM = Cu, Ag, and Au) and CO_2, as well as TM and NO_2, the electron density and Laplacian values of the critical points (CPs) of TM–O and TM–N bonds in $(CO_2)(TM)N_{20}(C_2B_2)_{30}^+$ and $(N_2O)(TM)N_{20}(C_2B_2)_{30}^+$ are calculated and listed in Table S1 (see the ESI†). The electron density and Laplacian values of the CPs of TM–O and TM–N bonds are in the range of 0.03–0.07 and 0.16–0.37, respectively, indicating that the TM–O and TM–N bonds are ionic bonds.[43]

4. Conclusions

A high-symmetry cage-like molecule $N_{20}(C_2B_2)_{30}$, resembling the fullerene C_{20} structurally, has been constructed by taking C_2B_2 and N motifs as linkers and nodes, respectively, and its stability and reactivity for cycloaddition and adsorption reactions are further demonstrated using density functional theory (DFT) calculations and AIMD simulations. The calculated results show that three cycloaddition reactions of $N_{20}(C_2B_2)_{30}$ with butadiene, cyclopentadiene, and diazomethane are all exothermic, and the corresponding free energy barriers are 20.9, 20.6, and 14.6 kcal mol^{-1}, respectively, showing that these reactions are feasible, both thermodynamically and kinetically. For the adsorption reactions, the carbon atoms of the inverted C=C bond in $N_{20}(C_2B_2)_{30}$ can effectively bind with H_2, CO, NO, and NO_2, whereas the boron atom site only accommodates CO. After the modification with transition metal (TM) ions

(Cu^+, Ag^+, and Au^+), CO_2 and N_2O can bind at the TM site of the obtained complexes $(TM)N_{20}(C_2B_2)_{30}^+$. Among these transition metal complexes, only $AuN_{20}(C_2B_2)_{30}^+$ shows obviously different adsorption energies for CO_2 and N_2O, and may be applied to effectively separate these two gas molecules. The present findings for novel structure and reactivity of $N_{20}(C_2B_2)_{30}$ may endow it with potential for applications in materials chemistry.

Author contributions

All authors contributed to the writing of the manuscript and approved the final version of the manuscript.

Data availability

The data supporting this article have been included as part of the ESI.†

Conflicts of interest

There are no conflicts to declare.

Notes and references

1 H. C. Longuet-Higgins and M. D. Roberts, *Proc. R. Soc. London, Ser. A*, 1955, **230**, 110–119.
2 A. R. Pitochelli and F. M. Hawthorne, *J. Am. Chem. Soc.*, 1960, **82**, 3228–3229.
3 J. A. Wunderlich and W. N. Lipscomb, *J. Am. Chem. Soc.*, 1960, **82**, 4427–4428.
4 X. Zhao, Z. Yang, H. Chen, Z. Wang, X. Zhou and H. Zhang, *Coord. Chem. Rev.*, 2021, **444**, 214042.
5 H. W. Kroto, J. R. Heath, S. C. O'Brien, R. F. Curl and R. E. Smalley, *Nature*, 1985, **318**, 162–163.
6 K. M. Kadish and R. Ruoff, *Fullerenes: Chemistry, Physics, and Technology*, Wiley-VCH, New York, 2000.
7 A. W. Hains, Z. Liang, M. A. Woodhouse and B. A. Gregg, *Chem. Rev.*, 2010, **110**, 6689–6735.
8 S. Goodarzi, T. Da Ros, J. Conde, F. Sefat and M. Mozafari, *Mater. Today*, 2017, **20**, 460–480.
9 G. Speranza, *Nanomaterials*, 2021, **11**, 967.
10 T. Suzuki, Q. Li, K. C. Khemani, F. Wudl and O. Almarsson, *Science*, 1991, **254**, 1186.
11 T. Suzuki, Q. Li, K. C. Khemani and F. Wudl, *J. Am. Chem. Soc.*, 1992, **114**, 7301–7302.
12 F. Wudl, *Acc. Chem. Res.*, 1992, **25**, 157–161.
13 A. B. Smith, R. M. Strongin, L. Brard, G. T. Furst, W. J. Romanow, K. G. Owens and R. C. King, *J. Am. Chem. Soc.*, 1993, **115**, 5829–5830.

This journal is © the Owner Societies 2025

Phys. Chem. Chem. Phys., 2025, **27**, 4246–4252 | **4251**

14 Q. Sun, Q. Wang, P. Jena and Y. Kawazoe, *J. Am. Chem. Soc.*, 2005, **127**, 14582–14583.

15 R. N. Goyal, V. K. Gupta, N. Bachheti and R. A. Sharma, *Electroanalysis*, 2008, **20**, 757–764.

16 J. Zheng, L. Huang, C.-H. Cui, Z.-C. Chen, X.-F. Liu, X. Duan, X.-Y. Cao, T.-Z. Yang, H. Zhu, K. Shi, P. Du, S.-W. Ying, C.-F. Zhu, Y.-G. Yao, G.-C. Guo, Y. Yuan, S.-Y. Xie and L.-S. Zheng, *Science*, 2022, **376**, 288–292.

17 N. Gonzalez Szwacki, A. Sadrzadeh and B. I. Yakobson, *Phys. Rev. Lett.*, 2007, **98**, 166804.

18 E. Scuseria, *Chem. Phys. Lett.*, 1991, **176**, 423–427.

19 A. D. Zdetsis, *Phys. Rev. B*, 2007, **76**, 075402.

20 K. Geng, T. He, R. Liu, S. Dalapati, K. T. Tan, Z. Li, S. Tao, Y. Gong, Q. Jiang and D. Jiang, *Chem. Rev.*, 2020, **120**, 8814–8933.

21 J. Jian, W. Li, X. Wu and M. Zhou, *Chem. Sci.*, 2017, **8**, 4443–4449.

22 Y. Zhao and D. G. Truhlar, *Theor. Chem. Acc.*, 2008, **120**, 215–241.

23 D. Andrae, U. Häußermann, M. Dolg, H. Stoll and H. Preuß, *Theor. Chim. Acta*, 1990, **77**, 123–141.

24 Y. Duan, C. Wu, S. Chowdhury, M. C. Lee, G. Xiong, W. Zhang, R. Yang, P. Cieplak, R. Luo, T. Lee, J. Caldwell, J. Wang and P. Kollman, *J. Comput. Chem.*, 2003, **24**, 1999–2012.

25 S. F. Boys and F. Bernardi, *Mol. Phys.*, 2002, **100**, 65–73.

26 E. D. Glendening, C. R. Landis and F. Weinhold, *J. Comput. Chem.*, 2019, **40**, 2234–2241.

27 T. Lu and F. Chen, *J. Comput. Chem.*, 2012, **33**, 580–592.

28 W. Humphrey, A. Dalke and K. Schulten, *J. Mol. Graphics*, 1996, **14**, 33–38.

29 P. V. R. Schleyer, C. Maerker, A. Dransfeld, H. Jiao and N. J. R. Van Eikema Hommes, *J. Am. Chem. Soc.*, 1996, **118**, 6317–6318.

30 M. J. Frisch, G. W. Trucks, H. B. Schlegel, G. E. Scuseria, M. A. Robb, J. R. Cheeseman, G. Scalmani, V. Barone, G. A. Petersson, H. Nakatsuji, X. Li, M. Caricato, A. V. Marenich, J. Bloino, B. G. Janesko, R. Gomperts, B. Mennucci, H. P. Hratchian, J. V. Ortiz, A. F. Izmaylov, J. L. Sonnenberg Williams, F. Ding, F. Lipparini, F. Egidi, J. Goings, B. Peng, A. Petrone, T. Henderson, D. Ranasinghe, V. G. Zakrzewski, J. Gao, N. Rega, G. Zheng, W. Liang, M. Hada, M. Ehara, K. Toyota, R. Fukuda, J. Hasegawa, M. Ishida, T. Nakajima, Y. Honda, O. Kitao, H. Nakai, T. Vreven, K. Throssell, J. A. MontgomeryJr, J. E. Peralta, F. Ogliaro, M. J. Bearpark, J. J. Heyd, E. N. Brothers, K. N. Kudin, V. N. Staroverov, T. A. Keith, R. Kobayashi, J. Normand, K. Raghavachari, A. P. Rendell, J. C. Burant, S. S. Iyengar, J. Tomasi, M. Cossi, J. M. Millam, M. Klene, C. Adamo, R. Cammi, J. W. Ochterski, R. L. Martin, K. Morokuma, O. Farkas, J. B. Foresman and D. J. Fox, *Gaussian 16, Revision A.03*, Gaussian Inc., Wallingford, CT, 2016.

31 G. Kresse and J. Hafner, *Phys. Rev. B*, 1993, **47**, 558–561.

32 M. Torrent, N. A. W. Holzwarth, F. Jollet, D. Harris, N. Lepley and X. Xu, *Comput. Phys. Commun.*, 2010, **181**, 1862–1867.

33 J. P. Perdew, K. Burke and M. Ernzerhof, *Phys. Rev. Lett.*, 1996, **77**, 3865–3868.

34 S. Nosé, *J. Chem. Phys.*, 1984, **81**, 511–519.

35 B. J. Levandowski and K. N. Houk, *J. Am. Chem. Soc.*, 2016, **138**, 16731–16736.

36 C. Zhang, W. Sun and Z. Cao, *J. Chem. Phys.*, 2007, **126**, 144306.

37 B. N. Cyvin, E. Brendsdal, J. Brunvoll and S. J. Cyvin, *J. Mol. Struct.*, 1995, **352**, 481–488.

38 G. Duškesas and S. Larsson, *Theor. Chem. Acc.*, 1997, **97**, 110–118.

39 C. Zhang and F. Li, *J. Phys. Chem. A*, 2012, **116**, 9123–9130.

40 C. Zhang, Z. Wang, J. Song, C. Li and Y. Mo, *Theor. Chem. Acc.*, 2019, **138**, 106.

41 Z. Tian, C. Zhang, Z. Pei, J. Liang and Y. Mo, *Mol. Syst. Des. Eng.*, 2023, **8**, 85–91.

42 C. Cao, C. Zhang, J. Gu and Y. Mo, *Phys. Chem. Chem. Phys.*, 2024, **26**, 28082–28090.

43 S. Shaik, D. Danovich, W. Wu and P. C. Hiberty, *Nat. Chem.*, 2009, **1**, 443–449.

44 S. Shaik, D. Danovich, J. M. Galbraith, B. Braïda, W. Wu and P. C. Hiberty, *Angew. Chem., Int. Ed.*, 2020, **59**, 984–1001.

45 H. Ueno, H. Kawakami, K. Nakagawa, H. Okada, N. Ikuma, S. Aoyagi, K. Kokubo, Y. Matsuo and T. Oshima, *J. Am. Chem. Soc.*, 2014, **136**, 11162–11167.

46 L. Wang, C. Lin, I. Boldog, J. Yang, C. Janiak and J. Li, *Angew. Chem., Int. Ed.*, 2024, **63**, e202317435.